

# Reachability Analysis for Feed-Forward Neural Networks using Face Lattices

Xiaodong Yang<sup>1</sup>, Hoang-Dung Tran<sup>1</sup>, Weiming Xiang<sup>2</sup>, and Taylor Johnson<sup>1</sup>

<sup>1</sup> Vanderbilt University, Nashville, TN 37212, USA

{xiaodong.yang, dung.h.tran, taylor.johnson}@vanderbilt.edu

<sup>2</sup> Augusta University, Augusta, GA 30912

xiangwming@gmail.com

**Abstract.** Deep neural networks have been widely applied as an effective approach to handle complex and practical problems. However, one of the most fundamental open problems is the lack of formal methods to analyze the safety of their behaviors. To address this challenge, we propose a parallelizable technique to compute exact reachable sets of a neural network to an input set. Our method currently focuses on feed-forward neural networks with ReLU activation functions. One of the primary challenges for polytope-based approaches is identifying the intersection between intermediate polytopes and hyperplanes from neurons. In this regard, we present a new approach to construct the polytopes with the face lattice, a complete combinatorial structure. The correctness and performance of our methodology are evaluated by verifying the safety of ACAS Xu networks and other benchmarks. Compared to state-of-the-art methods such as Reluplex, Marabou, and NNV, our approach exhibits a significantly higher efficiency. Additionally, our approach is capable of constructing the complete input set given an output set, so that any input that leads to safety violation can be tracked.

**Keywords:** Reachability analysis · Neural network · Formal verification.

## 1 Introduction

Deep neural networks (DNNs) have been playing a critical role in handling complex and practical problems and are being widely applied in safety-critical, autonomous cyber-physical systems (CPS). However, one major obstacle in realizing autonomous CPS is the lack of formal methods to provide guarantees on functional behaviors, such as in safety-critical systems like autonomous motor vehicles and robotic surgery machines. A slight perturbation in the input of a neural network may lead to an error behavior in output [13]. Recently, there has been significant effort to develop methods to establish robustness and formal guarantees of learning-enabled components (LECs) like DNNs [14,6,3,1,8,23,24,21,25,16,17,20,18,19]. There are two primary classes of reachability methodologies to formally analyze DNNs, over-approximation and exact (or complete) analysis. The over-approximation methods are mainly based on mixed-integer linear programs (MILPs) [11,1,10], zonotopes [3], abstract domain [17], and linearization [22,25]. These methods can only guarantee the soundness of the analysis but not completeness. The MILPs-based work [1] can guarantee both aspects when

neural networks have only one output, but fails when they have multiple outputs. Because it estimates the range of outputs independently and eventually generates a box domain that over approximates exact reachable sets. Most of the over-approximation methods are capable of efficiently analyzing large scales neural networks based ReLU activation functions. Their main strategy is replacing each ReLU function with a more conservative domain so that the number of output reachable sets of each layer can be largely reduced. But these approaches are only limited to point-wise inputs with a very little perturbation, and their conservativeness of the estimated reachable sets will exponentially grow as the input domain increases. This is already studied in [19].

While the exact analysis is mainly based on the satisfiability modulo theory (SMT) [8,9], polytopes [23] and Star set in a tool named NNV [19]. Through these approaches, both soundness and completeness of the verification can be guaranteed. The strategy of Reluplex [8] is extending the simplex method to handle the piece-wise linear ReLU activation function by allowing variables of defined ReLU pairs to temporarily violate their semantics. The Marabou [9] is an improved version of Reluplex. It supports arbitrary piecewise-linear activation function, parallel computation, etc. Another work ReluVal [21] is based on interval arithmetic to over approximate the bounds on the outputs. The influence of each input variable on the output is analyzed so that it can repeatedly split the input intervals and efficiently refine the output range. All these works focus on the satisfiability problem that is to determine whether there exists output that locates in the unsafe domain. While the works [23,19] are conducting the reachability analysis of a neural network. Given an input set, they can compute the exact output sets of a neural network. This reachability analysis is also associated with the quantification of linear regions of neural networks [12,15,4]. A linear region of a piecewise linear functions  $F : \mathbb{R}^n \rightarrow \mathbb{R}^m$  refers to a maximum convex subset of an input set in  $\mathbb{R}^n$ , on which the function  $F$  is linear. Accordingly, the input set is splitted by the ReLU function in each neuron into pieces which are linear regions. Each output set of a network computed by [23,19] corresponds to the output with respect to a linear region. Therefore, the number of output sets computed is equal to the number of linear regions. These methods can provide a full understanding of the neural network’s behavior and are promising directions towards safe networks.

However, improvement of the efficiency is challenging. The work [23] is constructing the input set with a polytope. It has three basic operations when a polytope passes through one layer of a neural network. They are respectively, *affine transformation* by the weight matrix and bias vector between layers, *intersection and division* by hyperplanes from the non-differentiable point at 0 in ReLU function of each neuron, and *projection* on the hyperplane due to the property of the negative domain in ReLU function. One of the primary challenges is to identify the intersection of a polytope with a hyperplane. To solve this problem, they use  $H$ -representation ( $H$ -rep) which is a set of linear inequalities to check the feasibility with another linear inequality from the hyperplane. This computation is treated as a linear programming problem. For the *affine transformation* and *projection*, the  $H$ -rep is transformed to  $V$ -representation ( $V$ -rep) which is a set of vertices. However, the change between  $H$ -rep and  $V$ -rep are respectively a vertex enumeration problem and a facet enumeration problem in computational geometry, both of which have high computational complexity. Therefore, the constant representa-

tion switching and feasibility inspecting lead to undesirable efficiency. The work [19] proposed the Star set which can avoid the transformation between  $H$ -rep and the  $V$ -rep. Instead, it identifies the intersection using optimization. But a large number of neurons will yield too many optimization processes and therefore impact its efficiency.

As a complementary approach, we present a novel face-lattice-based and parallelizable methodology that is capable of the sound and complete reachability analysis with higher efficiency. This method currently focuses on feed-forward neural networks with ReLU activation. To overcome the challenge, we develop an intuitive approach that is to inspect the distribution of a polytope's vertices on the sides of the hyperplane. If vertices scatter on both sides of or on the hyperplane, the intersection happens. Otherwise, it doesn't. The following problem is how to identify polytopes and their vertices generated from this intersection so that their complete structure information can be maintained for future operations. Here, we introduce the face lattice to encode the complete combinatorial structure for polytopes and preserves the adjacency between faces of the polytope, so that those three types of operations on polytopes can be more efficiently conducted.

## 2 Preliminaries

### 2.1 Feedforward Neural Networks

A FNN consists of one input layer, multiple hidden layers, and one output layer. Each layer contains multiple neurons which are interconnected with neurons in the next layer by weights in a feed-forward way. The output of each neuron is associated with three components: its input weight  $\omega$ , input bias  $b$  and the activation function  $f$ , as shown in:

$$y_i = f\left(\sum_{j=1}^n \omega_{i,j}x_j + b_j\right)$$

where  $\omega_{ij}$  and  $b_j$  are respectively the weight and bias from the  $j$ th neuron of the previous layer to the  $i$ th neuron of the current layer, and  $x_j$  is an input to this neuron and also the output of  $j$ th neuron in the front layer, and  $y_i$  is the output of the  $i$ th neuron. In this paper, we consider the ReLU activation which is defined as  $ReLU(x) = \max(0, x)$ . Let  $W_{(k,k-1)}$ ,  $b_k$  denote the weight matrix, the bias vector between the  $(k-1)$ th layer and  $k$ th layer, and  $X_{k-1}$  be its input consisting of elements  $x_j$ , then the output of the  $k$ th layer will be

$$\Phi_k(X_k) = ReLU(W_{(k,k-1)}X_k + b_k) \quad (1)$$

For the first hidden layer, its input  $X_0$  is also the input to the network. Besides, the output of one layer is also an input of the next layer. Therefore, given an input  $X_0$ , the output  $Y_k$  of the  $k$ th hidden layer will be

$$Y_k = \Phi_k(\Phi_{k-1}(\dots(\Phi_1(X_0)))) \quad (2)$$

### 2.2 Face Lattices

The geometric background of the face lattice structure is introduced in this section. It includes the concepts of supporting hyperplane, faces of polytopes as well as the properties of this structure. More other geometric details can be found in work [5].

**Definition 1 (Supporting Hyperplane).** A hyperplane  $\mathcal{H}$  denoted by  $\mathbf{a}^\top \mathbf{x} = b$  is supporting polytope  $P$  if one of its closed halfspaces,  $\mathbf{a}^\top \mathbf{x} \leq b$  or  $\mathbf{a}^\top \mathbf{x} \geq b$  contains  $P$ .

**Definition 2 (Face).** The face of a convex polytope is an intersection of this polytope with a supporting hyperplane. When the polytope is full dimensional, the face is named a nontrivial face. The polytope itself and the empty set are also its faces which are called trivial faces. When the dimension of  $\text{aff}(P \cap \mathcal{H})$  is  $k$ , the face is denoted as  $k$ -f or  $k$ -face. The function  $\text{aff}(S)$  indicates the affine hull of  $S$ , which is the smallest affine set that contains  $S$ .

A  $d$ -dimensional convex polytope  $P$  is called full dimensional if it locates in  $\mathbb{R}^{n=d}$ , otherwise it is not full dimensional if it is in  $\mathbb{R}^{n>d}$ . The convex polytope  $P$  consists of different dimensional faces. Regardless of  $P$ 's dimension and the space it locates in, it contains a set of 0-faces, 1-faces,  $\dots$ ,  $(d-2)$ -faces,  $(d-1)$ - faces as well as the empty set and itself. The 0-face, 1-face,  $(d-2)$ -face and  $(d-1)$ - face are respectively named *vertex*, *edges*, *ridges* and *facets*.

The face lattice  $\mathcal{L}(P)$  is a complete combinatorial structure that contains all faces of  $P$  and partially orders them by face containment. One face  $\mathcal{H}_i$  is said to contain a face  $\mathcal{H}_j$  if the  $\mathcal{H}_j$  is a subset of the  $\mathcal{H}_i$ . A tetrahedron and its face lattice are shown in (a) and (b) of Figure 1. The empty face  $\emptyset$  is not considered for a conciser presentation. Besides the 3-face which is the tetrahedron itself, there are 14 faces described by blue blocks and their dimension ranges from 0 to 2. The face containment only consider higher-dimensional faces containing adjacent lower-dimensional faces. For instance, the 1- $f_1$  (*edge*<sub>2-3</sub>) contains 0- $f_2$  (*vertex*<sub>2</sub>) and 0- $f_3$  (*vertex*<sub>3</sub>), and the 1- $f_1$  is contained in 2- $f_1$  (*plane*<sub>2-3-4</sub>) and 2- $f_2$  (*plane*<sub>1-2-3</sub>). The containment relation is expressed in a grey connection line. All the polytopes refer to convex polytopes that are expressed in the face lattice structure in the following sections

### 3 Operations of Polytopes

As discussed in the introduction, there are three basic operations in processing polytopes in the neural network. In terms of the sequential order, they are respectively, the *affine transformation* by weights, *intersection and division* by a hyperplane  $\mathcal{H}$ , and the *projection* on  $\mathcal{H}$ . The affine transformation is mapping the current polytope to another space. The combinatorial theory considers polytopes that differ only by a change of coordinates (an affine transformation) are equivalent [5]. The main reason is that the *affine transformation* only changes vertices but preserve polytopes' combinatorial structure. Therefore, its face lattice stays unchanged under this transformation. The *projection* on a hyperplane is orthogonally mapping the polytope on this hyperplane. Similarly to the affine transformation, it only works on its vertices. The rest of this section only focuses on the *intersection and division*.

#### 3.1 Intersection of Face Lattices with Hyperplanes

Since the face lattice contains all the information of faces adjacency, determination of an intersection between a polytope  $P$  and a hyperplane  $\mathcal{H}$  can be simplified to finding the

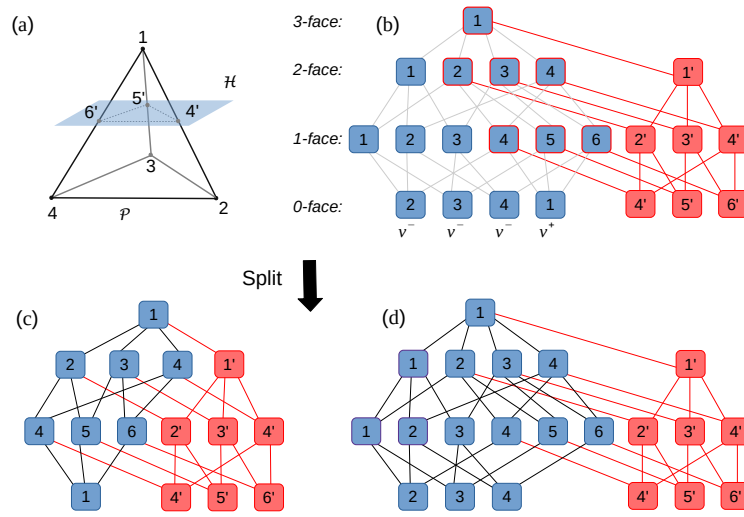


Fig. 1: A demonstration of the face lattice of a tetrahedron  $P$  and its *intersection and division*, by a hyperplane  $\mathcal{H}$ . In (b), the blocks filled with blue and connected by grey lines is its face lattice which structure is based on the Hasse diagram. The number of each entry represents the face's dimension. The grey connection only allows that high-dimensional faces contain low-dimensional faces. The blocks with red frames and blue color are the faces intersecting with  $\mathcal{H}$  in  $P$ , which are extracted from *positive* and *negative* vertices in terms of the Lemma 1. The face lattice of new generated faces is in red, which is extracted according to the Lemma 2. The red connection between blue blocks and red blocks denote the containment relation between faces in  $P$  and new faces. (c) and (d) represent the face lattice of the *positive* and *negative* polytopes, respectively.

intersection of edges in  $P$  with  $\mathcal{H}$ . It then can be realized by checking the distribution of edges' vertices on the side of  $\mathcal{H}$ . Let the  $\mathcal{H}$  be described by  $\mathbf{a}^\top \mathbf{x} + b = 0$ . To compute the vertices' distribution, we can substitute the  $\mathbf{x}$  with vertices. Let vertices such that  $\mathbf{a}^\top \mathbf{x}$  are greater than 0, smaller than 0, and equal to 0 be respectively called *positive* vertices  $v^+$ , *negative* vertices  $v^-$ , and *zero* vertices  $v^0$ . Accordingly, there are three cases in the *intersection and division*:

- (1) There exist both  $v^+$  and  $v^-$ . In this case, the hyperplane  $\mathcal{H}$  intersects with  $P$ , and a set of new faces  $S_f^*$  of dimensions between 0 and  $(d-1)$  are generated, where  $f \subseteq \mathcal{H}$  and  $f \subseteq P$  for all  $f \in S_f^*$ . The original polytope is thus divided into two non-empty sub-polytopes  $P_{sub}^+$  which consists of nonnegative vertices, and  $P_{sub}^-$  which consists of nonpositive vertices.
- (2) There are no  $v^-$ s. In such cases, polytope  $P$  is contained in the closed halfspace  $\mathbf{a}^\top \mathbf{x} \geq 0$ . The sub-polytopes  $P_{sub}$  generated from this operation is the  $P$  itself. It is a positive polytope  $P_{sub}^+$ .

- (3) There are no  $v^+$ s. In such cases, polytope  $P$  is contained in the closed halfspace  $\mathbf{a}^\top \mathbf{x} \leq 0$ . The sub-polytopes  $P_{sub}$  generated from this operation is also the  $P$  itself. It is a negative polytope  $P_{sub}^-$ .

Here we focus on the first case where the intersection occurs. To identify those two sub-polytopes, we first need to find the faces of  $P$  that yield the  $S_f^*$  in the intersection. Edges with both *positive* and *negative* vertices or at least having one *zero* vertex are said to have intersection with the hyperplane  $\mathcal{H}$ . In terms of the Lemma 1, higher-dimensional faces that also intersect with the  $\mathcal{H}$  can be identified from these edges. Thus all faces of  $P$  that intersect with  $\mathcal{H}$  are obtained. Intersecting with  $\mathcal{H}$ , each of such face will generate a new face that is one-dimension lower. These new faces the  $S_f^*$ . The process is demonstrated in the (b) of Figure 1. For instance, the 2- $f_2$  (*plane*<sub>1.2.3</sub>) intersects with  $\mathcal{H}$  and generates a new face 1- $f_{2'}$  (*edge*<sub>4'.5'</sub>) whose vertices 0- $f_{4'}$  (*vertex*<sub>4'</sub>) and 0- $f_{5'}$  (*vertex*<sub>5'</sub>) are respectively generated from the intersection of  $\mathcal{H}$  with 1- $f_4$  (*edge*<sub>1.2</sub>) and 1- $f_5$  (*edge*<sub>1.3</sub>).

Lemma 2 states that the face containment relation of the new faces  $S_f^*$  is inherited from faces' in the polytope. An example is shown in (b) of Figure 1. The red blocks represent the new faces set  $S_f^*$ , and the red connection between the red blocks represent the inherited face containment relation. For instance, the relation that the new face 1- $f_{3'}$  (*edge*<sub>5'.6'</sub>) contains the new face 0- $f_{6'}$  (*vertex*<sub>6'</sub>) is derived from the relation that 2- $f_3$  (*plane*<sub>1.3.4</sub>) contains 1- $f_6$  (*edge*<sub>1.4</sub>) in  $P$ . Overall, these two steps in *intersection* generate a new face lattice that includes all the faces of  $P$  and all the new generated faces  $S_f^*$ . Then as shown in (c) and (d), the *division* is splitting this face lattice into the  $P_{sub}^+$  and  $P_{sub}^-$  according to vertices.

**Lemma 1.** *If a  $k$ - $f$  ( $k$ -dimensional face) intersects with a hyperplane  $\mathcal{H}$ , all the  $(k+1)$ - $f$ s where  $k$ - $f \subseteq (k+1)$ - $f$  also intersect with  $\mathcal{H}$ .*

*Proof.*  $k$ - $f \subseteq (k+1)$ - $f$  indicates  $k$ - $f \cap \mathcal{H} \subseteq (k+1)$ - $f \cap \mathcal{H}$ . Since  $k$ - $f \cap \mathcal{H} \neq \emptyset$ , then  $(k+1)$ - $f \cap \mathcal{H} \neq \emptyset$ . Therefore,  $(k+1)$ - $f$  also intersect with  $\mathcal{H}$ .

**Lemma 2.** *Given two faces  $k$ - $f$  and  $(k+1)$ - $f$  where  $k$ - $f \subseteq (k+1)$ - $f$ , and that they both intersect with a hyperplane  $\mathcal{H}$  where  $k$ - $f \cap \mathcal{H} = (k-1)$ - $f'$  and  $(k+1)$ - $f \cap \mathcal{H} = k$ - $f'$ , then  $(k-1)$ - $f' \subseteq k$ - $f'$ .*

*Proof.*  $k$ - $f \subseteq (k+1)$ - $f$  indicates  $k$ - $f \cap \mathcal{H} \subseteq (k+1)$ - $f \cap \mathcal{H}$ . Therefore,  $(k-1)$ - $f' \subseteq k$ - $f'$  can be derived.

## 4 Reachability Analysis with Face Lattices

In this section, we use  $\mathcal{I}_k$  and  $\mathcal{O}_k$  to represent the input and output polytope sets of the  $k$ th layer. By substituting the  $X_k$  with  $\mathcal{I}_k$ , and the output with  $\mathcal{O}_k$  in the Equation 1, we obtain

$$\mathcal{O}_k = ReLU(W_{(k,k-1)}\mathcal{I}_k + b_k)$$

which indicates the three basic operations on polytopes. The operation on  $\mathcal{I}_k$  inside the parentheses is the *affine transformation*. The function  $ReLU(*)$  indicates a sequence

of *intersection and division*, and *projection* on the transformed polytope. As claimed in the abstract, our approach can derive the complete input set given an output set. It is realized by incorporating the transformation tuple in Definition 3 to maintain mathematical relation between an intermediate polytope  $P_k$  and a subset of the initial input  $P_0$  to the neural network. Thus, any violation of safe properties in output can be mapped back into the input. From the perspective of the *linear region* presented in Introduction section, the Equation 3 is one linear function and  $P_0^{sub}$  is one linear region.

**Definition 3 (Transformation Tuple).** Given an input polytope  $P_0$  to the neural network and a polytope  $P_k \in \mathcal{O}_k$ , a transformation tuple is denoted by  $P_k = \langle P_0^{sub}, M_k, d_k \rangle$  where  $P_0^{sub} \subseteq P_0$ , such that

$$P_k = M_k P_0^{sub} + d_k \quad (3)$$

#### 4.1 Processing of Transformation Tuple

Take the output computation of the first layer for example, suppose we have an initial input  $P_0$ , then its transformation tuple can be initialized as  $\langle P_0^{sub}, M_0, d_0 \rangle$  where  $P_0^{sub} = P_0$ ,  $M_0$  is an identity matrix, and  $d_0$  is an array of zeros. After the *affine transformation* by weights  $W_{(1,0)}$  and  $b_{(1,0)}$ , the  $P_0^{sub}$  stays unchanged and the tuple will be updated to  $\langle P_0^{sub}, M_1, d_1 \rangle$ , where

$$M_1 = W_{(1,0)} M_0, \quad d_1 = W_{(1,0)} d_0 + b_{(1,0)}. \quad (4)$$

Let  $P_1$  be this updated tuple. Afterwards, the *intersection and division* operation will be conducted on this new tuple for each neuron in this layer. Suppose we start by processing the first neuron, we can first derive a hyperplane  $\mathcal{H}_1 : \mathbf{a}_1^\top \mathbf{x} + c_1 = 0$  where  $\mathbf{a}_1$  is an array with its first element  $\mathbf{a}_1[1] = 1$  and the rest being zeros, and  $c_1 = 0$ . When considering the  $i$ th neuron, the  $\mathbf{a}_1[i] = 1$  and the rest keeps the same. According to the ReLU function, the subset of  $P_1$  that is in the closed halfspace  $\mathbf{a}_1^\top \mathbf{x} + c_1 \geq 0$  stays unchanged. For the subset that is in the closed halfspace  $\mathbf{a}_1^\top \mathbf{x} + c_1 \leq 0$ , all its  $\mathbf{x}[1]$  is set to 0. These subsets can be identified by the *intersection* operation. Instead of determining the intersection of  $P_1$  with  $\mathcal{H}_1$ , we choose to check the intersection of its  $P_0^{sub}$  with a mapped-back hyperplane  $\mathcal{H}_0$  from  $\mathcal{H}_1$  by Equation 5 and 6. This approach is directly operating the initial input subset  $P_0^{sub}$ , which is helpful for the further computation. Besides, the *intersection and division* on the  $P_0^{sub}$  is also the process of splitting and generating linear regions.

The method of mapping  $\mathcal{H}_1$  into the space of  $P_0^{sub}$  and obtaining  $\mathcal{H}_0$  is as following. From the Equation 3, we can derive that

$$\mathbf{x}_1 = M_1 \mathbf{x}_0^{sub} + d_1 \quad (5)$$

where  $\mathbf{x}_0^{sub} \in P_0^{sub}$  and  $\mathbf{x}_1 \in P_1$ . By combining this equation with  $\mathcal{H}_1$ , we have

$$\begin{aligned} \mathbf{a}_1^\top \mathbf{x}_1 + c_1 &= \mathbf{a}_1^\top (M_1 \mathbf{x}_0^{sub} + d_1) + c_1 \\ &= (\mathbf{a}_1^\top M_1) \mathbf{x}_0^{sub} + (\mathbf{a}_1^\top d_1 + c_1) = 0 \end{aligned} \quad (6)$$

Thus, we can obtain the mapped hyperplane  $\mathcal{H}_0 : \mathbf{a}_0^\top \mathbf{x}_0^{sub} + c_0 = 0$ , where  $\mathbf{a}_0^\top = \mathbf{a}_1^\top M_1$  and  $c_0 = \mathbf{a}_1^\top d_1 + c_1$ .

During the *intersection and division* operation, the processing of the tuple depends on different cases. In the first case,  $P_0^{sub}$  will be splitted into two polytopes  $P_0^{sub+}$  and  $P_0^{sub-}$  by the hyperplane  $\mathcal{H}_0$ . Correspondingly, the original tuple of  $P_1$  will also be splitted and we achieve

$$P_1^+ = \langle P_0^{sub+}, M_1, d_1 \rangle, P_1^- = \langle P_0^{sub-}, M_1, d_1 \rangle$$

According to the property of the ReLU function,  $P_1^+$  stays unchanged and no *projection* operation is needed. While the points of the  $P_1^-$  should be mapped to the  $\mathcal{H}_1$  where the first element  $\mathbf{x}[1]$  of them will be changed to zero. As shown in the following equation, this operation can be realized by left multiplying  $I_1$  with  $P_1^-$  where  $I_1$  is an identify matrix with the first diagonal entry being zero. When processing with the  $i$ th neuron,  $I_i$  will be an identify matrix with  $i$ th diagonal entry being zero.

$$\begin{aligned} P_1'^- &= I_1 P_1^- = I_1 (M_1 P_0^{sub-} + d_1) \\ &= (I_1 M_1) P_0^{sub-} + (I_1 d_1) \end{aligned} \quad (7)$$

After the *projection*, the  $P_1'^- = \langle P_0^{sub-}, M_1', d_1' \rangle$ , where

$$M_1' = I_1 M_1, d_1' = I_1 d_1. \quad (8)$$

While in the second case, only  $P_0^{sub+}$  is generated from the *intersection and division* on  $P_0^{sub}$ . Then  $P_0^{sub+} = P_0^{sub}$  and no *projection* operation is needed. In the third case, only  $P_0^{sub-}$  is generated where  $P_0^{sub-} = P_0^{sub}$ . The *projection* is applied though Equation 7 and 8. Overall, the first case yields two intermediate polytopes  $P_1^+$  and  $P_1'^-$ . The second and third cases respectively yields  $P_1 = \langle P_0^{sub}, M_1, d_1 \rangle$  and  $P_1 = \langle P_0^{sub}, M_1', d_1' \rangle$ .

This process is computing the output of one neuron, which is denoted by  $\mathbb{N}(\ast)$  in Equation 9. Afterward, these output polytopes will be the input to the next neuron, This process is repeated until all the neurons in the first layer are considered. Then the polytopes obtained are the output of the first layer. The computing output of one layer to its inputs is denoted by  $\mathbb{L}(\ast)$ . For a formal description, let  $\mathbb{N}_j^{[k]}$  represent the sequence of *affine transformation*, *intersection and division*, and *projection* for the  $j$ th neuron in the  $k$ th layer, and  $\mathcal{S}_k$  be the output set of this layer with respect to an input set to this layer, then we have

$$\mathcal{S}_k = \mathbb{N}_m^{[k]}(\mathbb{N}_{m-1}^{[k]}(\dots(\mathbb{N}_1^{[k]}(\mathcal{S}_{k-1})))) \quad (9)$$

. Let  $\mathbb{L}_k$  be the process of Equation 9, and  $\mathcal{O}_k$  be the output of the  $k$ th layer to an input  $P_0$  to the network, then we have

$$\mathcal{O}_k = \mathbb{L}_k(\mathbb{L}_{[k-1]}(\dots(\mathbb{L}_1(P_0)))) \quad (10)$$

## 4.2 Mapping Back to Input

Let the unsafe range of output be a set of halfspaces  $\mathcal{H}_{us} : \mathbf{a}_u^\top \mathbf{x} + c_u \leq 0$ . Suppose we have an output polytope  $P_k = \langle P_0^{sub}, M_k, d_k \rangle$ . Similarly with the Equation 5, we have

$$\mathbf{x}_k = M_k \mathbf{x}_0^{sub} + d_k$$



**Algorithm 1** Reachable set computation of a neural network

---

**Input:**  $n, P_0$  # layer index, input polytope  
**Output:**  $\mathcal{O}_n$  # reachable set of the  $n$ th layer

- 1: **procedure**  $\mathcal{O}_n = \text{LAYEROUTPUT}(n, P_0)$
- 2:    $\mathcal{I}_k = P_0$  #  $\mathcal{I}_k$ : input set to the  $k$ th layer
- 3:   **for**  $k = 1 : n$  **do**
- 4:      $\mathcal{O}_k = \text{empty}$  #  $\mathcal{O}_k$ : output set of the  $k$ th layer
- 5:     **for (parfor)**  $P$  in  $\mathcal{I}_k$  **do**
- 6:        $\mathcal{S}_k = \text{singleLayerOutput}(k, P)$
- 7:       add  $\mathcal{S}_k$  to  $\mathcal{O}_k$
- 8:      $\mathcal{I}_k = \mathcal{O}_k$
- 9:   **return**  $\mathcal{O}_n = \mathcal{O}_k$
- 10: **procedure**  $\mathcal{S}_k = \text{SINGLELAYEROUTPUT}(k, P)$
- 11:    $\mathcal{S}_k = \text{linearTransform}(k, P)$
- 12:   **for**  $i = 1 : m$  **do** #  $m$ : the number of neurons
- 13:      $\mathcal{S}_{temp} = \text{empty}$
- 14:     **for**  $P'$  in  $\mathcal{S}_k$  **do**
- 15:        $P'^+, P'^- = \text{intersectDivide}(i, P')$
- 16:       **if**  $P'^-$  is not none **then**
- 17:          $P'^- = \text{projectionHyperplane}(i, P'^-)$
- 18:       add  $P'^+, P'^-$  to  $\mathcal{S}_{temp}$
- 19:      $\mathcal{S}_k = \mathcal{S}_{temp}$
- 20:   **return**  $\mathcal{S}_k$

---

By combining  $\mathcal{H}_{us}$  with this equation, we can derive that

$$\begin{aligned} \mathbf{a}_u^\top \mathbf{x}_k + c_u &= \mathbf{a}_u^\top (M_k \mathbf{x}_0^{sub} + d_k) + c_u \\ &= (\mathbf{a}_u^\top M_k) \mathbf{x}_0^{sub} + (\mathbf{a}_u^\top d_k + c_u) \leq 0 \end{aligned} \quad (11)$$

and that  $\mathbf{a}_0^\top = \mathbf{a}_u^\top M_k$  and  $c_0 = \mathbf{a}_u^\top d_k + c_u$  are parameters of the mapped halfspace in the  $P_0^{sub}$ 's space. To determine unsafety, we can check the existence of vertices that are contained in the mapped halfspaces. To extract the unsafe set in the input  $P_0$ , we can apply a series of the *intersection and division* operations to the  $P_0^{sub}$ 's (linear regions) with the  $\mathcal{H}_{us}$ . Negative polytopes generated from such operation are the input sets that violate the safety requirement.

### 4.3 Parallelizable Algorithm

Two potential parallelizable algorithms are proposed in this section based on the fact that input polytopes to one network layer are independent. One is processing in parallel all the input polytopes to one layer until all their output is completed, and then repeating

this procedure to the following layers until the final output of the neural network is achieved. This strategy is described in Algorithm 1 where it is parallelized by replacing **for** with **parfor** in Line 5. To simplify this presentation, we assume that the output layer of neural networks is also with ReLU function. Accordingly, when  $n$  is the number of layers in the neural network, the output of this algorithm is the final reachable set of the neural network. The description of functions are as following:

- (1) **layerOutput()** corresponds to the Equation 10. The  $\mathcal{S}_k$  and  $\mathcal{O}_k$  corresponds to the symbols in Equation 9 and 10, respectively.
- (2) **singleLayerOutput()** corresponds to the Equation 9.
- (3) **linearTransform()** corresponds to the Equation 4. The  $P$  is an element polytope, and the  $\mathcal{S}_k$  is initialized with the transformed  $P$ .
- (4) **intersectDivide()** corresponds to the operation of *intersection and division*. by a hyperplane as shown in the (b), (c) and (d) of Figure 1. Its output are one *positive* sub-polytope  $P'^+$  and one *negative* sub-polytope  $P'^-$ .
- (5) **projectionHyperplane()** corresponds to the projection of the *negative* sub-polytopes on a hyperplane determined by the  $i$ th neuron, as shown in Equation 7.

---

**Algorithm 2** Alternative parallel algorithm
 

---

[tb]

**Input:**  $n, P_0$  # layer index, input polytope**Output:**  $\mathcal{O}_n$  # reachable set of the  $n$ th layer

```

1: procedure  $\mathcal{O}_n = \text{REACHCOMPUTE}(n, P_0)$ 
2:    $\mathcal{O}_j = \text{layerOutput}(j, P_0)$  # function in Algorithm 1
3:   parfor  $P$  in  $\mathcal{O}_j$  do
4:      $\mathcal{I}_k = P$ 
5:     for  $k = j : n$  do
6:        $\mathcal{O}_k = \text{empty}$ 
7:       for  $P'$  in  $\mathcal{I}_k$  do
8:          $\mathcal{S}_k = \text{singleLayerOutput}(k, P')$ 
9:         add  $\mathcal{S}_k$  to  $\mathcal{O}_k$ 
10:       $\mathcal{I}_k = \mathcal{O}_k$ 
11:    add  $\mathcal{O}_k$  to  $\mathcal{O}_n$ 
12:   return  $\mathcal{O}_n$ 

```

---

However, when programmed in Python using its embedded **multiprocessing** package, this parallel algorithm will suffer from a computational burden due to copying the parent process memory in the computation of each layer. It means that when the function **singleLayerOutput()** is invoked in parallel, the memory in the parent process will be copied to those multiple created children processes. This memory copying occurs in each network layer and leads to an extra-large computational burden. This phenomenon is significant when there is a large number of polytopes in  $\mathcal{I}_k$ .

Therefore, an alternative method is inherited from the first one to handle that situation. Instead of processing polytopes in parallel in each layer, we choose to start processing them in parallel from a specific layer. The details are illustrated in Algorithm 2. It first computes the output polytopes of the  $j$  layer to the input  $P_0$  by invoking the function **layerOutput** in Algorithm 1. Then, the algorithm from Line 3 to the end will be executed. In this process, the memory copying only happens once in Line 3 with a relatively smaller number of polytopes in  $\mathcal{O}_j$ . Therefore, it outperforms Algorithm 1. For the complexity, the maximum number of output sets that both of algorithms can compute for a network with total  $m$  hidden neurons and one input set is  $2^m$ . In practice, the actual number is much smaller since the *intersection and division* doesn't really split intermediates polytopes in every neuron.

## 5 Evaluation

### 5.1 Safety Verification of ACAS Xu Networks

In this section, we evaluate our method against the Reluplex, Marabou, and NNV. They are currently well-known approaches that also do the exact reachability analysis of feed-forward neural networks with ReLU activation functions. The evaluation task is to verify the safety of ACAS Xu networks in [7]. Given an input domain and an unsafe domain, Reluplex and Marabou solve the satisfiability problem, which is they only determine if there are outputs satisfying unsafe conditions. While our method and NNV are computing all the exact reachable sets of the output and then determining their intersection with the unsafe area.

The ACAS Xu networks are used to approximate a large lookup table that converts sensor measurements into maneuver advisories in an Airborne Collision Avoidance System so that the massive memory occupation by the table and the lookup time can be reduced. The set of networks contain 45 fully-connected DNNs for different combinations of discretized parameters. Each one has five inputs, five outputs, and six hidden layers. Each layer consists of fifty neurons with ReLU activation functions. Therefore there are 300 hidden neurons total in each network. The five inputs consist of the sensor measurements: (1)  $\rho$ : Distance from ownship to intruder; (2)  $\theta$ : Angle to intruder relative to ownship heading direction; (3)  $\psi$ : Heading angle of intruder relative to ownship heading direction; (4)  $v_{own}$ : Speed of ownship; (5)  $v_{int}$ : Speed of intruder. The outputs are advisory scores for five different actions, where the lowest score corresponds to the best action. The five actions are respectively, clear of conflict (COC), weak right, strong right, weak left, and strong left. There are ten safety properties  $\phi_1, \dots, \phi_{10}$  which specify input bounds and linear constraints on the output. The details can be found in the Appendix of [8].

In the experiment, All the 45 networks are tested on Property 1,2,3 and 4. The hardware configuration is Intel Core i7-6700 CPU @3.4GHz×8 Processor, 64 GB Memory, 64-bit Ubuntu 18.04<sup>3</sup>. The summary of results are shown in Table 1. The details are shown in Table 3,4,5 and 6 in Appendix. In the implementation, Marabou DNC, NNV, ReluVal and our method that support parallel computation are all assigned with

<sup>3</sup> Codes are available online at <https://github.com/verivital/FaceLattice>

8 processors. While Reluplex and Marabou is implemented in a nonparallel way. The following is the evaluation of each method:

- **Reluplex**: As the summary indicates, Reluplex exhibits a relatively lower efficiency compared to other methods. Besides, an incorrect result is found in our implementation. The test on the *network<sub>17</sub>* and Property 2 identifies an adversarial input that generates an output  $[-0.00, 0.30, 0.18, 0.19, 0.20]$ . While the desired output for Property 2 is that the score for COC (the first element of output) is not maximum. Clearly, this output doesn't violate this condition.
- **Marabou**: For the performance of Marabou, It shows an improvement in the efficiency compared to Reluplex. But It still takes a significant time to complete tasks. Its scalability to larger and deeper neural networks is unclear.
- **Marabou DnC**: It is a divide-and-conquer solving mode of the Marabou, where the input range is partitioned into sub-ranges. Compared to Reluplex and Marabou, it shows a higher efficiency on Property 1 and 2. However, it fails to outperform them on Property 3 and 4. This performance inconsistency is related to its configuration. Its configuration consists of parameters such as initial-divides and online divides flags which are the number of times to bisect the input region. Such parameters can greatly affect performance. Besides, their optimal selection differs between different networks. Therefore, their optimal performance can't be always achieved. The parameters we applied for this implementation are the default values.
- **ReluVal**: Compared to other tools, it exhibits a higher efficiency in some cases such as Property 1, but it can be very slow in other cases such as Property 2. Its performance is also inconsistent. ReluVal is constructed with two modes, CHECK\_ADV\_MODE and CHECK\_NORM\_MODE. The first mode can quickly breathe search for counter-examples but it can't guarantee to identify them if they truly exist. While the second mode can return adversarial examples if exist but its high efficiency can't be guaranteed. As recommended by their authors, The first mode is applied in the beginning. For those tasks without finding adversarial examples, the second mode is then applied. But the performance of the second mode can be greatly affected by its parameters in the configuration. For instance, the parameter "depth" indicates from which depth the algorithm should start checking adversarial examples. Its optimal value also differs between networks. Thus, its optimal performance can't be guaranteed. The parameters we utilized are default values for this experiment.
- **NNV Exact Star**: It shows high efficiency in Property 3 and 4 but fails to complete most of the tasks in Property 1 and 2. As introduced in the beginning, this inconsistency is probably related to the optimization processes involved in the computation of output sets.
- **Face Lattice**: Our method shows a relatively higher and more consistent efficiency. In Property 1, our method fails to outperform ReluVal because we compute the exact output sets first and then solve the satisfiability problem while the large input range of Property 1 yields a significant number of linear regions to compute. However, the output sets obtained from the test on Property 1 can be reused for Property 2 where networks have the same output reachable sets.

In addition to the high efficiency, our approach can also visualize the exact reachability of a neural network so that an intuitive inspection can first be conducted for safety

Methods	ACAS XU $\phi_1$				ACAS XU $\phi_2$			
	SAT	UNSAT	TIMEOUT	TIME	SAT	UNSAT	TIMEOUT	TIME
Reluplex	0	28	17	> 462208	40	3	2	> 153292
Marabou	0	38	7	> 335933	39	3	3	> 160024
Marabou DnC	0	45	0	99754	39	4	2	> 89294
ReluVal	0	45	0	467	39	6	0	28019
NNV Exact Star	0	14	31	> 711271	10	4	31	> 370
Our Method	0	45	0	31312	39	6	0	255

Methods	ACAS XU $\phi_3$				ACAS XU $\phi_4$			
	SAT	UNSAT	TIMEOUT	TIME	SAT	UNSAT	TIMEOUT	TIME
Reluplex	3	42	0	28454	3	42	0	11880
Marabou	3	42	0	19466	3	42	0	8470
Marabou DnC	3	41	1	> 56322	3	42	0	25110
ReluVal	3	42	0	759	3	42	0	56
NNV Exact Star	3	42	0	7457	3	42	0	1157
Our Method	3	42	0	511	3	42	0	296

Table 1: Summary of the performance of each method on Property 1,2,3 and 4. The SAT means there exists output that satisfies the unsafe condition, which indicates that the neural network is unsafe. While the UNSAT means that there doesn’t exist such output, which indicates the network is safe. The TIMEOUT is set to 5h for all the tasks. The TIME represents the total running time (seconds) of one method on 45 networks.

properties. An example of the exact reachable set of the network  $N_{4,7}$  is demonstrated in Figure 2, whose lower bound and upper bound of the input are  $[1500, -0.06, 3.1, 1000, 700]$  and  $[1800, 0.06, 3.14, 1200, 800]$ . Additionally, 2000 random inputs are sampled to demonstrate the method’s correctness. The reachable sets are visualized separately in two figures. With such output sets, we can verify different safety properties, instead of running the algorithm repeatedly for each property as Reluplex and Marabou do. Besides, our method can also compute the exact input set that leads to property violations. For instance, the inputs that make the network  $N_{1,2}$  violate Property2 are computed as shown in Figure 3. It is a union of 104 polytopes. The element belonging to these polytopes will yield property violations. For the element that doesn’t belong to them but are contained in the input range, they won’t cause any violation.

## 5.2 Reachability Analysis of Microbenchmarks

To further evaluate our approach, we compare them on a set of microbenchmarks that are proposed in work [2]. These benchmarks consisting of neural networks are created from two different sources. The networks  $N_2-N_4$  are trained with some analytical functions. While the networks  $N_{11}-N_{14}$  come from the unwindings of a closed-loop

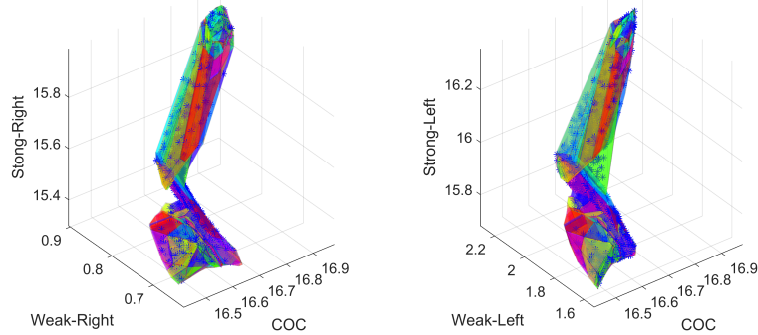


Fig. 2: Exact reachable set of the network  $N_{4,7}$  on Property 4. The blue star points are the output w.r.t. 2000 random input samples. They all locate on or inside the output sets.

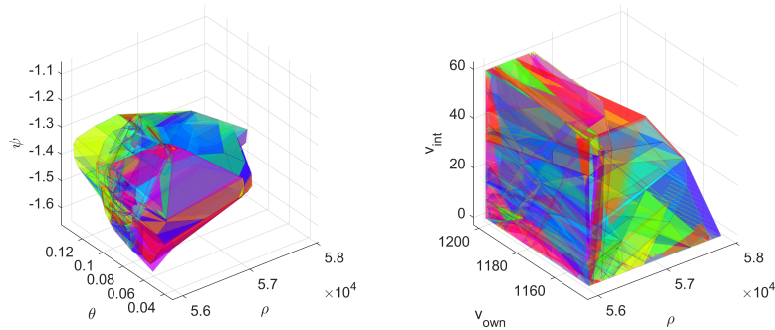


Fig. 3: Complete input sets that lead to the property  $\phi_2$  violation on the network  $N_{1,2}$ . It is a union of 104 polytopes.

controller and a plant model. Here we check these networks’ safety on some synthetic unsafe domains. Only Marabou DnC and NNV are considered because they support parallel computation. ReluVal is not included as we are not able to apply ReluVal to these new networks. Problems have been reported to the author but haven’t been solved. For the networks  $N_2$ - $N_4$  which have only one hidden layer, we equally partition the input range for our method and NNV into 1024 subsets, so that the parallel computation can be applied. The details of each benchmark and the performance of each approach are shown in Table 2. Most of the networks consist of thousands of neurons. Dealing with such a large size of networks, our approach also exhibits a high efficiency. While other methods fail to complete all the tasks.

ID				Our Method		Marabou DnC	NNV	
	$x$	$k$	$m$	$N_p$	$time$	$time$	$N_p$	$time$
$N_2$	2	1	500	16760	25	36	16760	635
$N_3$	2	1	500	4339	8	15	4339	53
$N_4$	2	1	1000	192709	803	157	×	TIMEOUT
$N_{11}$	3	9	1427	25312	449	TIMEOUT	25312	1824
$N_{12}$	3	14	2292	25312	837	TIMEOUT	25312	1690
$N_{13}$	3	19	3057	462833	20033	TIMEOUT	×	TIMEOUT
$N_{14}$	3	24	3822	236062	13991	TIMEOUT	×	TIMEOUT

Table 2: Performance results on microbenchmarks. The label  $x$ ,  $k$  and  $m$  respectively denote the number of input, the number of layers and total number of ReLU neurons.  $N_p$  is the number of output reachable sets and  $time(second)$  is the running time. The TIMEOUT is set to 10 hours.

## 6 Conclusion and Future Work

The exact reachability analysis of neural networks is a hard problem, but it is essential to conducting robustness verification. In this paper, we presented a polytope-based and parallelizable method to conduct exact reachability analysis of the feed-forward neural networks with ReLU activation. Instead of using the  $H$  and  $V$  representations, we construct polytopes with the face lattice, a structure encoding complete combinatorial information. Through comparing to state-of-the-art methods like Reluplex, Marabou, NNV, and ReluVal, we can verify its correctness and high efficiency. As discussed, the exact reachable set can be reusable for different properties. The comparison includes the verification of a set of real-world ACAS Xu neural networks and the reachability computation of some other benchmarks. To improve the efficiency and convenience, we can also partition a wide-range input into smaller subsets and build a library for their reachable sets so that further analysis of any input contained in such range can be reduced to merely looking up the library. Overall, there are multiple directions to improve our approach. In the future, we plan to explore more concise and efficient polytope representations than the face lattice because it becomes complicated for high dimensional polytopes. Another potential enhancement is to detect the polytopes in the input set that determine the output range so that the redundant polytopes can be ignored and the computation burden can be reduced. Additionally, we also consider extending our approach to convolutional neural networks (CNNs) in the future.

## References

1. Dutta, S., Jha, S., Sanakaranarayanan, S., Tiwari, A.: Output range analysis for deep neural networks. arXiv preprint arXiv:1709.09130 (2017)
2. Dutta, S., Jha, S., Sankaranarayanan, S., Tiwari, A.: Output range analysis for deep feed-forward neural networks. In: NASA Formal Methods Symposium. pp. 121–138. Springer (2018)
3. Gehr, T., Mirman, M., Drachler-Cohen, D., Tsankov, P., Chaudhuri, S., Vechev, M.: Ai2: Safety and robustness certification of neural networks with abstract interpretation. In: 2018 IEEE Symposium on Security and Privacy (SP). pp. 3–18. IEEE (2018)
4. Hanin, B., Rolnick, D.: Complexity of linear regions in deep networks. arXiv preprint arXiv:1901.09021 (2019)
5. Henk, M., Richter-Gebert, J., Ziegler, G.M.: 16 basic properties of convex polytopes. Handbook of discrete and computational geometry pp. 255–382 (2004)
6. Huang, X., Kwiatkowska, M., Wang, S., Wu, M.: Safety verification of deep neural networks. In: International Conference on Computer Aided Verification. pp. 3–29. Springer (2017)
7. Julian, K.D., Lopez, J., Brush, J.S., Owen, M.P., Kochenderfer, M.J.: Policy compression for aircraft collision avoidance systems. In: Digital Avionics Systems Conference (DASC), 2016 IEEE/AIAA 35th. pp. 1–10. IEEE (2016)
8. Katz, G., Barrett, C., Dill, D.L., Julian, K., Kochenderfer, M.J.: Reluplex: An efficient smt solver for verifying deep neural networks. In: International Conference on Computer Aided Verification. pp. 97–117. Springer (2017)
9. Katz, G., Huang, D.A., Ibeling, D., Julian, K., Lazarus, C., Lim, R., Shah, P., Thakoor, S., Wu, H., Zeljić, A., et al.: The marabou framework for verification and analysis of deep neural networks. In: International Conference on Computer Aided Verification. pp. 443–452. Springer (2019)
10. Kouvaros, P., Lomuscio, A.: Formal verification of cnn-based perception systems. arXiv preprint arXiv:1811.11373 (2018)
11. Lomuscio, A., Maganti, L.: An approach to reachability analysis for feed-forward relu neural networks. arXiv preprint arXiv:1706.07351 (2017)
12. Montufar, G.F., Pascanu, R., Cho, K., Bengio, Y.: On the number of linear regions of deep neural networks. In: Advances in neural information processing systems. pp. 2924–2932 (2014)
13. Moosavi-Dezfooli, S.M., Fawzi, A., Frossard, P.: Deepfool: a simple and accurate method to fool deep neural networks. In: Proceedings of the IEEE Conference on Computer Vision and Pattern Recognition. pp. 2574–2582 (2016)
14. Pulina, L., Tacchella, A.: An abstraction-refinement approach to verification of artificial neural networks. In: International Conference on Computer Aided Verification. pp. 243–257. Springer (2010)
15. Serra, T., Tjandraatmadja, C., Ramalingam, S.: Bounding and counting linear regions of deep neural networks. arXiv preprint arXiv:1711.02114 (2017)
16. Singh, G., Gehr, T., Mirman, M., Püschel, M., Vechev, M.: Fast and effective robustness certification. In: Advances in Neural Information Processing Systems. pp. 10825–10836 (2018)
17. Singh, G., Gehr, T., Püschel, M., Vechev, M.: An abstract domain for certifying neural networks. Proceedings of the ACM on Programming Languages **3**(POPL), 41 (2019)
18. Tran, H.D., Musau, P., Lopez, D.M., Yang, X., Nguyen, L.V., Xiang, W., Johnson, T.T.: Parallelizable reachability analysis algorithms for feed-forward neural networks. In: Proceedings of the 7th International Workshop on Formal Methods in Software Engineering. pp. 31–40. IEEE Press (2019)



19. Tran, H.D., Musau, P., Lopez, D.M., Yang, X., Nguyen, L.V., Xiang, W., Johnson, T.T.: Star-based reachability analysis for deep neural networks. In: 23rd International Symposium on Formal Methods (FM'19). Springer International Publishing (October 2019)
20. Wang, S., Pei, K., Whitehouse, J., Yang, J., Jana, S.: Efficient formal safety analysis of neural networks. In: Advances in Neural Information Processing Systems. pp. 6369–6379 (2018)
21. Wang, S., Pei, K., Whitehouse, J., Yang, J., Jana, S.: Formal security analysis of neural networks using symbolic intervals. In: 27th {USENIX} Security Symposium ({USENIX} Security 18). pp. 1599–1614 (2018)
22. Weng, T.W., Zhang, H., Chen, H., Song, Z., Hsieh, C.J., Boning, D., Dhillon, I.S., Daniel, L.: Towards fast computation of certified robustness for relu networks. arXiv preprint arXiv:1804.09699 (2018)
23. Xiang, W., Tran, H., Johnson, T.: Reachable set computation and safety verification for neural networks with relu activations. arXiv preprint arXiv:1712.08163 (2017)
24. Xiang, W., Tran, H., Johnson, T.: Output reachable set estimation and verification for multi-layer neural networks. IEEE transactions on neural networks and learning systems (99), 1–7 (2018)
25. Zhang, H., Weng, T.W., Chen, P.Y., Hsieh, C.J., Daniel, L.: Efficient neural network robustness certification with general activation functions. In: Advances in Neural Information Processing Systems. pp. 4944–4953 (2018)

ID	Reluplex		Marabou		Marabou DnC		ReluVal		NNV Exact Star			Our Method		
	VT	V	VT	V	VT	V	VT	V	$N_p$	VT	V	$N_p$	VT	V
$N_{11}$	1875	UNSAT	393	UNSAT	74	UNSAT	0.17	UNSAT	39810	4203	UNSAT	39810	81.70	UNSAT
$N_{12}$	2697	UNSAT	802	UNSAT	129	UNSAT	0.31	UNSAT	45606	4912	UNSAT	45606	92.22	UNSAT
$N_{13}$	> 18000	×	2319	UNSAT	1040	UNSAT	2.92	UNSAT	114219	12665	UNSAT	114219	247.14	UNSAT
$N_{14}$	5953	UNSAT	2328	UNSAT	948	UNSAT	2.89	UNSAT	154449	15920	UNSAT	154449	305.15	UNSAT
$N_{15}$	3825	UNSAT	745	UNSAT	93	UNSAT	0.44	UNSAT	122275	12293	UNSAT	122275	232.20	UNSAT
$N_{16}$	2899	UNSAT	1003	UNSAT	95	UNSAT	0.28	UNSAT	×	> 18000	×	376352	703.66	UNSAT
$N_{17}$	1061	UNSAT	295	UNSAT	49	UNSAT	0.17	UNSAT	66388	6359	UNSAT	66388	150.14	UNSAT
$N_{18}$	3121	UNSAT	209	UNSAT	45	UNSAT	0.15	UNSAT	110085	11309	UNSAT	110085	242.49	UNSAT
$N_{19}$	731	UNSAT	116	UNSAT	33	UNSAT	0.15	UNSAT	135559	12393	UNSAT	135559	262.91	UNSAT
$N_{21}$	6796	UNSAT	1792	UNSAT	420	UNSAT	1.08	UNSAT	×	> 18000	×	193080	371.01	UNSAT
$N_{22}$	14272	UNSAT	3352	UNSAT	787	UNSAT	1.8	UNSAT	×	> 18000	×	471882	876.97	UNSAT
$N_{23}$	16001	UNSAT	4379	UNSAT	1134	UNSAT	2.92	UNSAT	×	> 18000	×	194168	356.67	UNSAT
$N_{24}$	3579	UNSAT	1208	UNSAT	214	UNSAT	0.95	UNSAT	114037	10796	UNSAT	114037	222.26	UNSAT
$N_{25}$	> 18000	×	15613	UNSAT	3741	UNSAT	6.57	UNSAT	×	> 18000	×	677346	1197.44	UNSAT
$N_{26}$	> 18000	×	12420	UNSAT	4168	UNSAT	5.00	UNSAT	×	> 18000	×	309365	600.91	UNSAT
$N_{27}$	9489	UNSAT	> 18000	×	3956	UNSAT	19.76	UNSAT	×	> 18000	×	679021	1256.58	UNSAT
$N_{28}$	> 18000	×	15692	UNSAT	3688	UNSAT	6.64	UNSAT	×	> 18000	×	585437	1078.93	UNSAT
$N_{29}$	> 18000	×	> 18000	×	5818	UNSAT	14.55	UNSAT	×	> 18000	×	909914	1671.80	UNSAT
$N_{31}$	1664	UNSAT	2367	UNSAT	463	UNSAT	0.73	UNSAT	×	> 18000	×	252573	467.78	UNSAT
$N_{32}$	4112	UNSAT	3076	UNSAT	647	UNSAT	1.30	UNSAT	×	> 18000	×	181291	330.25	UNSAT
$N_{33}$	3891	UNSAT	2384	UNSAT	419	UNSAT	2.08	UNSAT	×	> 18000	×	341409	614.31	UNSAT
$N_{34}$	4129	UNSAT	2629	UNSAT	362	UNSAT	0.98	UNSAT	133749	12569	UNSAT	133749	234.51	UNSAT
$N_{35}$	5905	UNSAT	5867	UNSAT	1861	UNSAT	2.63	UNSAT	×	> 18000	×	364948	645.07	UNSAT
$N_{36}$	> 18000	×	12864	UNSAT	3197	UNSAT	45.97	UNSAT	×	> 18000	×	1003429	1709.95	UNSAT
$N_{37}$	4489	UNSAT	15038	UNSAT	2990	UNSAT	21.01	UNSAT	×	> 18000	×	475107	860.52	UNSAT
$N_{38}$	> 18000	×	15371	UNSAT	2271	UNSAT	13.78	UNSAT	×	> 18000	×	472132	894.35	UNSAT
$N_{39}$	> 18000	×	12162	UNSAT	4261	UNSAT	18.14	UNSAT	×	> 18000	×	378803	701.68	UNSAT
$N_{41}$	> 18000	×	> 18000	×	975	UNSAT	30.45	UNSAT	×	> 18000	×	402334	772.64	UNSAT
$N_{42}$	8428	UNSAT	4875	UNSAT	1309	UNSAT	4.59	UNSAT	×	> 18000	×	484417	926.55	UNSAT
$N_{43}$	5038	UNSAT	3344	UNSAT	854	UNSAT	2.00	UNSAT	138104	14161	UNSAT	138104	256.62	UNSAT
$N_{44}$	4529	UNSAT	2662	UNSAT	303	UNSAT	1.60	UNSAT	143350	14960	UNSAT	143350	258.32	UNSAT
$N_{45}$	16149	UNSAT	5592	UNSAT	3152	UNSAT	5.68	UNSAT	×	> 18000	UNSAT	456909	821.95	UNSAT
$N_{46}$	> 18000	×	> 18000	×	4577	UNSAT	35.42	UNSAT	×	> 18000	×	1295596	2348.38	UNSAT
$N_{47}$	> 18000	×	> 18000	×	6857	UNSAT	38.00	UNSAT	×	> 18000	×	651996	1160.78	UNSAT
$N_{48}$	> 18000	×	16384	UNSAT	5095	UNSAT	62.31	UNSAT	×	> 18000	×	515006	902.38	UNSAT
$N_{49}$	> 18000	×	> 18000	×	15687	UNSAT	34.63	UNSAT	×	> 18000	×	984139	1815.10	UNSAT
$N_{51}$	2279	UNSAT	1501	UNSAT	265	UNSAT	0.89	UNSAT	×	> 18000	×	201660	396.82	UNSAT
$N_{52}$	7097	UNSAT	1948	UNSAT	416	UNSAT	1.14	UNSAT	×	> 18000	×	260741	490.51	UNSAT
$N_{53}$	2210	UNSAT	925	UNSAT	113	UNSAT	0.40	UNSAT	125749	12928	UNSAT	125749	232.37	UNSAT
$N_{54}$	4946	UNSAT	1985	UNSAT	425	UNSAT	1.08	UNSAT	81317	7796	UNSAT	81317	159.14	UNSAT
$N_{55}$	9043	UNSAT	5838	UNSAT	1991	UNSAT	2.34	UNSAT	×	> 18000	×	212854	403.67	UNSAT
$N_{56}$	> 18000	×	9412	UNSAT	4546	UNSAT	27.42	UNSAT	×	> 18000	×	621782	1133.41	UNSAT
$N_{57}$	> 18000	×	7109	UNSAT	1857	UNSAT	6.63	UNSAT	×	> 18000	×	355708	655.24	UNSAT
$N_{58}$	> 18000	×	> 18000	×	4858	UNSAT	25.59	UNSAT	×	> 18000	×	544678	1023.01	UNSAT
$N_{59}$	> 18000	×	14729	UNSAT	3571	UNSAT	14.10	UNSAT	×	> 18000	×	619110	1147.20	UNSAT

Table 3: Property 1

ID	Reluplex		Marabou		Marabou DnC		ReluVal		NNV Exact Star			Our Method		
	VT	V	VT	V	VT	V	VT	V	$N_p$	VT	V	$N_p$	VT	V
$N_{11}$	4888	UNSAT	4290	UNSAT	1887	UNSAT	1.04	UNSAT	39810	9	UNSAT	39810	0.67	UNSAT
$N_{12}$	396	SAT	760	SAT	450	SAT	2.84	SAT	45606	11	SAT	45606	0.64	SAT
$N_{13}$	1704	SAT	1122	SAT	9465	SAT	5.55	SAT	114219	28	SAT	114219	1.82	SAT
$N_{14}$	881	SAT	56	SAT	4028	SAT	4.03	SAT	154449	38	SAT	154449	2.45	SAT
$N_{15}$	22	SAT	73	SAT	230	SAT	387.48	UNSAT	122275	30	SAT	122275	1.68	SAT
$N_{16}$	242	SAT	5493	SAT	961	SAT	10.65	SAT	×	×	×	376352	5.80	SAT
$N_{17}$	4759	SAT	9585	UNSAT	2847	UNSAT	11.19	UNSAT	66388	16	UNSAT	66388	1.04	UNSAT
$N_{18}$	15180	UNSAT	> 18000	×	12714	UNSAT	387.48	UNSAT	110085	27	UNSAT	110085	1.67	UNSAT
$N_{19}$	8211	UNSAT	16207	UNSAT	5667	UNSAT	18.07	UNSAT	135559	33	UNSAT	135559	2.18	UNSAT
$N_{21}$	614	SAT	51	SAT	67	SAT	0.08	SAT	×	×	×	193080	2.71	SAT
$N_{22}$	14	SAT	39	SAT	62	SAT	0.075	SAT	×	×	×	471882	7.33	SAT
$N_{23}$	68	SAT	745	SAT	111	SAT	0.05	SAT	×	×	×	194168	2.61	SAT
$N_{24}$	46	SAT	182	SAT	17	SAT	0.04	SAT	114037	28	SAT	114037	1.81	SAT
$N_{25}$	382	SAT	620	SAT	504	SAT	0.05	SAT	×	×	×	677346	11.11	SAT
$N_{26}$	7024	SAT	1513	SAT	527	SAT	0.08	SAT	×	×	×	309365	4.41	SAT
$N_{27}$	6256	SAT	835	SAT	11	SAT	0.10	SAT	×	×	×	679021	11.04	SAT
$N_{28}$	1097	SAT	311	SAT	48	SAT	0.07	SAT	×	×	×	585437	9.21	SAT
$N_{29}$	9076	SAT	12676	SAT	3814	SAT	0.16	SAT	×	×	×	909914	15.01	SAT
$N_{31}$	939	SAT	1086	SAT	52	SAT	0.06	SAT	×	×	×	252573	3.59	SAT
$N_{32}$	1212	SAT	3083	SAT	829	SAT	0.12	SAT	×	×	×	181291	2.93	SAT
$N_{33}$	> 18000	×	> 18000	×	> 18000	×	6165.70	UNSAT	×	×	×	341409	5.29	UNSAT
$N_{34}$	2137	SAT	3618	SAT	407	SAT	0.04	SAT	133749	32	SAT	133749	2.21	SAT
$N_{35}$	5011	SAT	237	SAT	361	SAT	0.05	SAT	×	×	×	364948	5.70	SAT
$N_{36}$	239	SAT	1279	SAT	680	SAT	2.11	SAT	×	×	×	1003429	14.56	SAT
$N_{37}$	746	SAT	855	SAT	2165	SAT	0.66	SAT	×	×	×	475107	6.36	SAT
$N_{38}$	601	SAT	5647	SAT	1273	SAT	0.06	SAT	×	×	×	472132	7.49	SAT
$N_{39}$	81	SAT	436	SAT	582	SAT	0.04	SAT	×	×	×	378803	5.16	SAT
$N_{41}$	801	SAT	464	SAT	380	SAT	0.06	SAT	×	×	×	402334	5.39	SAT
$N_{42}$	> 18000	×	> 18000	×	> 18000	×	7842.15	UNSAT	×	×	×	484417	6.61	UNSAT
$N_{43}$	16	SAT	428	SAT	239	SAT	0.08	SAT	138104	33	SAT	138104	2.21	SAT
$N_{44}$	120	SAT	319	SAT	43	SAT	0.07	SAT	143350	35	SAT	143350	2.23	SAT
$N_{45}$	5090	SAT	9689	SAT	432	SAT	0.06	SAT	×	×	×	456909	6.87	SAT
$N_{46}$	1795	SAT	2683	SAT	498	SAT	0.04	SAT	×	×	×	1295596	19.50	SAT
$N_{47}$	5087	SAT	700	SAT	384	SAT	0.03	SAT	×	×	×	651996	9.55	SAT
$N_{48}$	5503	SAT	1402	SAT	48	SAT	0.05	SAT	×	×	×	515006	7.16	SAT
$N_{49}$	7147	SAT	3275	SAT	62	SAT	0.07	SAT	×	×	×	984139	14.33	SAT
$N_{51}$	2331	SAT	191	SAT	56	SAT	0.04	SAT	×	×	×	201660	2.73	SAT
$N_{52}$	458	SAT	45	SAT	16	SAT	0.07	SAT	×	×	×	260741	3.68	SAT
$N_{53}$	89	SAT	5028	SAT	274	SAT	13524.38	SAT	125749	30	SAT	125749	1.73	SAT
$N_{54}$	50	SAT	57	SAT	361	SAT	0.08	SAT	81317	20	SAT	81317	1.12	SAT
$N_{55}$	1212	SAT	1881	SAT	112	SAT	0.04	SAT	×	×	×	212854	3.40	SAT
$N_{56}$	2679	SAT	635	SAT	149	SAT	0.05	SAT	×	×	×	621782	9.25	SAT
$N_{57}$	1879	SAT	3300	SAT	9	SAT	0.03	SAT	×	×	×	355708	5.62	SAT
$N_{58}$	7894	SAT	253	SAT	324	SAT	0.04	SAT	×	×	×	544678	8.34	SAT
$N_{59}$	3315	SAT	4875	SAT	148	SAT	0.03	SAT	×	×	×	619110	8.79	SAT

Table 4: Property 2

ID	Reluplex		Marabou		Marabou DnC		ReluVal		NNV Exact Star			Our Method		
	VT	V	VT	V	VT	V	VT	V	$N_p$	VT	V	$N_p$	VT	V
$N_{11}$	6156	UNSAT	3637	UNSAT	> 18000	×	176.89	UNSAT	70631	1463	UNSAT	70631	110.89	UNSAT
$N_{12}$	4942	UNSAT	3418	UNSAT	3221	UNSAT	4.30	UNSAT	39529	1026	UNSAT	39529	65.63	UNSAT
$N_{13}$	1134	UNSAT	1795	UNSAT	10858	UNSAT	6.91	UNSAT	12274	299	UNSAT	12274	20.17	UNSAT
$N_{14}$	528	UNSAT	187	UNSAT	186	UNSAT	0.53	UNSAT	4275	52	UNSAT	4275	8.74	UNSAT
$N_{15}$	317	UNSAT	124	UNSAT	193	UNSAT	0.28	UNSAT	4744	84	UNSAT	4744	9.35	UNSAT
$N_{16}$	64	UNSAT	37	UNSAT	23	UNSAT	0.13	UNSAT	1266	20	UNSAT	1266	3.53	UNSAT
$N_{17}$	1	SAT	5	SAT	6	SAT	0.03	SAT	500	6	SAT	500	1.20	SAT
$N_{18}$	3	SAT	2	SAT	6	SAT	0.03	SAT	393	5	SAT	393	0.99	SAT
$N_{19}$	2	SAT	2	SAT	6	SAT	0.03	SAT	290	3	SAT	290	0.75	SAT
$N_{21}$	1208	UNSAT	1001	UNSAT	813	UNSAT	34.56	UNSAT	16179	336	UNSAT	16179	25.00	UNSAT
$N_{22}$	653	UNSAT	480	UNSAT	2106	UNSAT	15.13	UNSAT	6861	126	UNSAT	6861	10.51	UNSAT
$N_{23}$	1043	UNSAT	1103	UNSAT	1163	UNSAT	5.99	UNSAT	10614	203	UNSAT	10614	17.18	UNSAT
$N_{24}$	41	UNSAT	22	UNSAT	8	UNSAT	0.99	UNSAT	345	5	UNSAT	345	0.92	UNSAT
$N_{25}$	235	UNSAT	58	UNSAT	13	UNSAT	0.72	UNSAT	2456	34	UNSAT	2456	4.69	UNSAT
$N_{26}$	79	UNSAT	23	UNSAT	8	UNSAT	0.053	UNSAT	253	4	UNSAT	253	0.84	UNSAT
$N_{27}$	116	UNSAT	57	UNSAT	9	UNSAT	0.38	UNSAT	1199	17	UNSAT	1199	2.46	UNSAT
$N_{28}$	83	UNSAT	13	UNSAT	8	UNSAT	0.08	UNSAT	326	5	UNSAT	326	0.97	UNSAT
$N_{29}$	27	UNSAT	2	UNSAT	7	UNSAT	0.02	UNSAT	188	2	UNSAT	188	0.61	UNSAT
$N_{31}$	177	UNSAT	97	UNSAT	240	UNSAT	5.12	UNSAT	5967	118	UNSAT	5967	10.10	UNSAT
$N_{32}$	1561	UNSAT	1973	UNSAT	1564	UNSAT	11.13	UNSAT	36967	907	UNSAT	36967	61.91	UNSAT
$N_{33}$	1105	UNSAT	344	UNSAT	891	UNSAT	0.50	UNSAT	7848	193	UNSAT	7848	14.38	UNSAT
$N_{34}$	209	UNSAT	106	UNSAT	34	UNSAT	0.90	UNSAT	2077	46	UNSAT	2077	4.51	UNSAT
$N_{35}$	83	UNSAT	41	UNSAT	10	UNSAT	10.65	UNSAT	1034	16	UNSAT	1034	2.30	UNSAT
$N_{36}$	255	UNSAT	120	UNSAT	194	UNSAT	223.05	UNSAT	1857	37	UNSAT	1857	4.10	UNSAT
$N_{37}$	35	UNSAT	8	UNSAT	7	UNSAT	0.22	UNSAT	107	2	UNSAT	107	0.33	UNSAT
$N_{38}$	179	UNSAT	57	UNSAT	25	UNSAT	7.50	UNSAT	654	10	UNSAT	654	1.68	UNSAT
$N_{39}$	118	UNSAT	55	UNSAT	35	UNSAT	5.10	UNSAT	1201	21	UNSAT	1201	2.25	UNSAT
$N_{41}$	201	UNSAT	94	UNSAT	914	UNSAT	15.93	UNSAT	2276	43	UNSAT	2276	4.71	UNSAT
$N_{42}$	2882	UNSAT	1724	UNSAT	11861	UNSAT	174.28	UNSAT	17894	444	UNSAT	17894	28.83	UNSAT
$N_{43}$	1767	UNSAT	1257	UNSAT	1014	UNSAT	4.37	UNSAT	20746	618	UNSAT	20746	36.90	UNSAT
$N_{44}$	86	UNSAT	19	UNSAT	8	UNSAT	0.21	UNSAT	560	8	UNSAT	560	1.38	UNSAT
$N_{45}$	35	UNSAT	14	UNSAT	8	UNSAT	0.19	UNSAT	351	4	UNSAT	351	0.72	UNSAT
$N_{46}$	300	UNSAT	118	UNSAT	55	UNSAT	0.30	UNSAT	2496	61	UNSAT	2496	5.83	UNSAT
$N_{47}$	126	UNSAT	54	UNSAT	43	UNSAT	0.81	UNSAT	944	13	UNSAT	944	2.39	UNSAT
$N_{48}$	142	UNSAT	36	UNSAT	41	UNSAT	3.53	UNSAT	576	9	UNSAT	576	1.37	UNSAT
$N_{49}$	143	UNSAT	33	UNSAT	22	UNSAT	0.14	UNSAT	611	19	UNSAT	611	1.59	UNSAT
$N_{51}$	1131	UNSAT	764	UNSAT	1910	UNSAT	40.54	UNSAT	9461	180	UNSAT	9461	15.91	UNSAT
$N_{52}$	151	UNSAT	120	UNSAT	635	UNSAT	4.28	UNSAT	2104	40	UNSAT	2104	3.40	UNSAT
$N_{53}$	341	UNSAT	146	UNSAT	64	UNSAT	0.25	UNSAT	2874	41	UNSAT	2874	9.24	UNSAT
$N_{54}$	62	UNSAT	42	UNSAT	10	UNSAT	0.28	UNSAT	758	13	UNSAT	758	1.61	UNSAT
$N_{55}$	86	UNSAT	27	UNSAT	18	UNSAT	0.86	UNSAT	1305	19	UNSAT	1305	2.96	UNSAT
$N_{56}$	283	UNSAT	81	UNSAT	47	UNSAT	1.87	UNSAT	1143	21	UNSAT	1143	3.15	UNSAT
$N_{57}$	35	UNSAT	5	UNSAT	8	UNSAT	0.06	UNSAT	88	1	UNSAT	88	0.32	UNSAT
$N_{58}$	310	UNSAT	157	UNSAT	22	UNSAT	0.15	UNSAT	2368	42	UNSAT	2368	4.53	UNSAT
$N_{59}$	19	UNSAT	8	UNSAT	8	UNSAT	0.17	UNSAT	107	3	UNSAT	107	0.37	UNSAT

Table 5: Property 3

ID	Reluplex		Marabou		Marabou DnC		ReluVal		NNV Exact Star			Our Method		
	VT	V	VT	V	VT	V	VT	V	$N_p$	VT	V	$N_p$	VT	V
$N_{11}$	1291	UNSAT	1929	UNSAT	11379	UNSAT	1.90	UNSAT	19143	398	UNSAT	19143	33.09	UNSAT
$N_{12}$	1267	UNSAT	2012	UNSAT	8629	UNSAT	2.42	UNSAT	13143	258	UNSAT	13143	23.16	UNSAT
$N_{13}$	1150	UNSAT	956	UNSAT	2806	UNSAT	0.80	UNSAT	9837	200	UNSAT	9837	23.03	UNSAT
$N_{14}$	107	UNSAT	79	UNSAT	93	UNSAT	0.39	UNSAT	1184	15	UNSAT	1184	2.21	UNSAT
$N_{15}$	352	UNSAT	299	UNSAT	267	UNSAT	0.87	UNSAT	6608	138	UNSAT	6608	15.70	UNSAT
$N_{16}$	219	UNSAT	201	UNSAT	82	UNSAT	0.34	UNSAT	4443	72	UNSAT	4443	11.63	UNSAT
$N_{17}$	1	SAT	2	SAT	6	SAT	0.03	SAT	642	8	SAT	642	1.68	SAT
$N_{18}$	3	SAT	2	SAT	6	SAT	0.04	SAT	397	6	SAT	397	0.97	SAT
$N_{19}$	3	SAT	1	SAT	6	SAT	0.03	SAT	471	6	SAT	471	2.93	SAT
$N_{21}$	330	UNSAT	239	UNSAT	112	UNSAT	1.73	UNSAT	5066	86	UNSAT	5066	14.42	UNSAT
$N_{22}$	415	UNSAT	273	UNSAT	210	UNSAT	3.98	UNSAT	4500	80	UNSAT	4500	8.52	UNSAT
$N_{23}$	243	UNSAT	47	UNSAT	35	UNSAT	1.74	UNSAT	1087	15	UNSAT	1087	2.15	UNSAT
$N_{24}$	86	UNSAT	23	UNSAT	16	UNSAT	0.32	UNSAT	913	17	UNSAT	913	1.91	UNSAT
$N_{25}$	151	UNSAT	95	UNSAT	46	UNSAT	0.69	UNSAT	3419	66	UNSAT	3419	7.97	UNSAT
$N_{26}$	118	UNSAT	71	UNSAT	70	UNSAT	0.45	UNSAT	1462	28	UNSAT	1462	2.67	UNSAT
$N_{27}$	34	UNSAT	25	UNSAT	8	UNSAT	0.09	UNSAT	555	9	UNSAT	555	1.22	UNSAT
$N_{28}$	549	UNSAT	121	UNSAT	33	UNSAT	0.13	UNSAT	1805	41	UNSAT	1805	5.23	UNSAT
$N_{29}$	52	UNSAT	6	UNSAT	7	UNSAT	0.04	UNSAT	157	3	UNSAT	157	0.68	UNSAT
$N_{31}$	478	UNSAT	220	UNSAT	283	UNSAT	2.17	UNSAT	4281	73	UNSAT	4281	8.91	UNSAT
$N_{32}$	107	UNSAT	237	UNSAT	102	UNSAT	0.84	UNSAT	8708	147	UNSAT	8708	25.52	UNSAT
$N_{33}$	116	UNSAT	36	UNSAT	12	UNSAT	0.13	UNSAT	1201	18	UNSAT	1201	2.15	UNSAT
$N_{34}$	75	UNSAT	32	UNSAT	13	UNSAT	0.28	UNSAT	1214	21	UNSAT	1214	2.73	UNSAT
$N_{35}$	206	UNSAT	212	UNSAT	52	UNSAT	2.20	UNSAT	3630	100	UNSAT	3630	11.16	UNSAT
$N_{36}$	141	UNSAT	50	UNSAT	47	UNSAT	3.02	UNSAT	1495	28	UNSAT	1495	3.00	UNSAT
$N_{37}$	304	UNSAT	49	UNSAT	10	UNSAT	0.60	UNSAT	862	18	UNSAT	862	2.47	UNSAT
$N_{38}$	131	UNSAT	48	UNSAT	20	UNSAT	0.49	UNSAT	542	14	UNSAT	542	1.49	UNSAT
$N_{39}$	621	UNSAT	144	UNSAT	57	UNSAT	2.85	UNSAT	2684	68	UNSAT	2684	7.10	UNSAT
$N_{41}$	49	UNSAT	30	UNSAT	40	UNSAT	5.85	UNSAT	848	11	UNSAT	848	1.66	UNSAT
$N_{42}$	244	UNSAT	77	UNSAT	42	UNSAT	4.35	UNSAT	1348	25	UNSAT	1348	2.72	UNSAT
$N_{43}$	243	UNSAT	163	UNSAT	100	UNSAT	2.35	UNSAT	3725	53	UNSAT	3725	10.98	UNSAT
$N_{44}$	206	UNSAT	52	UNSAT	31	UNSAT	2.82	UNSAT	1253	25	UNSAT	1253	3.36	UNSAT
$N_{45}$	217	UNSAT	53	UNSAT	32	UNSAT	2.98	UNSAT	1255	18	UNSAT	1255	2.74	UNSAT
$N_{46}$	177	UNSAT	18	UNSAT	8	UNSAT	0.05	UNSAT	2366	41	UNSAT	2366	5.45	UNSAT
$N_{47}$	47	UNSAT	16	UNSAT	10	UNSAT	0.29	UNSAT	216	4	UNSAT	216	0.57	UNSAT
$N_{48}$	195	UNSAT	68	UNSAT	25	UNSAT	0.41	UNSAT	1591	30	UNSAT	1591	3.40	UNSAT
$N_{49}$	422	UNSAT	51	UNSAT	19	UNSAT	0.14	UNSAT	2566	40	UNSAT	1591	5.92	UNSAT
$N_{51}$	513	UNSAT	174	UNSAT	193	UNSAT	5.46	UNSAT	6932	104	UNSAT	6932	10.90	UNSAT
$N_{52}$	210	UNSAT	48	UNSAT	31	UNSAT	1.00	UNSAT	4361	71	UNSAT	4361	11.55	UNSAT
$N_{53}$	124	UNSAT	39	UNSAT	41	UNSAT	0.21	UNSAT	1662	27	UNSAT	1662	3.45	UNSAT
$N_{54}$	144	UNSAT	43	UNSAT	12	UNSAT	0.27	UNSAT	1088	18	UNSAT	1088	2.05	UNSAT
$N_{55}$	114	UNSAT	61	UNSAT	30	UNSAT	1.02	UNSAT	1549	27	UNSAT	1549	3.12	UNSAT
$N_{56}$	160	UNSAT	55	UNSAT	45	UNSAT	0.60	UNSAT	677	15	UNSAT	677	1.50	UNSAT
$N_{57}$	38	UNSAT	8	UNSAT	8	UNSAT	0.07	UNSAT	157	3	UNSAT	157	0.41	UNSAT
$N_{58}$	111	UNSAT	48	UNSAT	22	UNSAT	0.17	UNSAT	502	15	UNSAT	502	1.21	UNSAT
$N_{59}$	116	UNSAT	57	UNSAT	14	UNSAT	0.19	UNSAT	992	19	UNSAT	992	2.18	UNSAT

Table 6: Property 4